

Anharmonic phonon coupling in vapor-liquid-solid grown ZnO nanowires

A. Souidi, R. Lopez, Jr., R. D. Dawson, and Y. Gu^{a)}

Department of Physics and Astronomy, Washington State University, Pullman, Washington 99164, USA

(Received 9 September 2009; accepted 22 October 2009; published online 13 November 2009)

We have determined quantitatively third-order anharmonic phonon coupling matrix elements in vapor-liquid-solid (VLS) grown ZnO nanowires, via an analysis of the Raman line shape of the E_2^{high} phonon mode. The results suggest that the decay of the E_2^{high} phonon into the sum of two acoustic phonons is suppressed in VLS-grown ZnO nanowires compared to bulk ZnO. While further studies are needed to elucidate the origin of this phenomenon, we suggest that isotope effects on Zn vapor transport and diffusion through metal nanocatalysts, processes during the VLS growth, can be contributing mechanisms. © 2009 American Institute of Physics. [doi:10.1063/1.3263709]

In crystalline materials, the description of lattice vibrations and potentials is a critical issue in developing a fundamental understanding of charge carrier dynamics, thermal expansion and transport, mechanical deformations, and phase transformations. Particularly, anharmonic (cubic, quartic, or higher order) terms in the expansion of the lattice potential energy are of great importance. A manifestation of effects arising from these anharmonic terms is phonon-phonon interactions, the characteristics of which can thus provide insight into the anharmonicity of lattice vibrations. To this end, Raman spectroscopy is a powerful tool that enables direct access to phonon interactions.

Recently, semiconductor nanowires have been attracting much research interest due to their unique physical properties. Among these nanomaterials, ZnO nanowires have been demonstrated to exhibit enhanced mechanical strength¹ and Young's modulus,² unique structural phase transformations,³ as well as to enable highly efficient mechanical-to-electric energy conversions.⁴ The anharmonicity of lattices contributes significantly to the underlying mechanisms of these properties.

In this work, we have used Raman spectroscopy to investigate the anharmonic phonon coupling in ZnO nanowires grown by a vapor-liquid-solid (VLS) process. We have specifically focused on the E_2^{high} phonon mode that decays anharmonically via three-phonon processes.^{5,6} Through an analysis of the Raman phonon line shape, we have determined quantitatively third-order anharmonic phonon coupling matrix elements. The obtained values describe well the characteristics of variable-temperature (85–600 K) Raman spectra. The results indicate that the decay of the E_2^{high} phonon into the sum of two acoustic phonons is suppressed in VLS-grown ZnO nanowires compared to bulk ZnO. We suggest isotope effects on Zn vapor transport and diffusion through metal nanocatalysts, processes during the VLS growth, as possible contributing mechanisms.

ZnO nanowires (with diameters of ~ 30 nm) were grown via the VLS process with Au nanoparticles as the catalyst (details can be found in Ref. 7). Micro-Raman spectra were obtained using a Renishaw InVia Raman microscope with the laser excitation provided by 325 and 442 nm lines from a Kimmon He–Cd laser. For measurements at

temperatures from 85 K to the room temperature (RT), we used a liquid-helium microscopy cryostat (part of Cryo-View2000 from Nanonics); high-temperature experiments (up to 600 K) were performed using an Instec microscope hot stage (HCS302).

Transmission electron microscopy (TEM) images of a typical ZnO nanowire are shown in Fig. 1. A residual catalyst can be seen at the tip of the nanowire, consistent with the VLS growth. The obtained electron-diffraction patterns indicate a wurtzite structure with [0002] as the growth direction. No dislocations or planar defects were observed from nanowires investigated.

Figure 2(b) shows a RT Raman spectrum of the E_2^{high} phonon (solid line) obtained with the 442 nm excitation,⁸ which exhibits an asymmetric low-frequency broadening. This has been observed in bulk ZnO and attributed to anharmonic phonon interactions.⁶ While the isotopic disorder can also lead to such a broadening,⁹ it seems unlikely to be the origin here as the E_2^{high} phonon mode involves predominantly the motion of oxygen atoms (which are nearly isotopically pure). Moreover, the A_1 longitudinal optical (LO) phonon peak obtained with the 325 nm excitation (not shown here) exhibits a fairly symmetric line shape, excluding the lattice disorder as the dominant origin of the asymmetric broadening. This asymmetric line shape of the E_2^{high} phonon thus provides an opportunity to evaluate the anharmonic phonon coupling strength. In particular, the E_2^{high} phonon decays anharmonically into two acoustic phonon modes at $\omega_1 = 250 \text{ cm}^{-1}$ and $\omega_2 = 190 \text{ cm}^{-1}$, as well as into a difference between an optical phonon and an acoustic phonon at ω_3

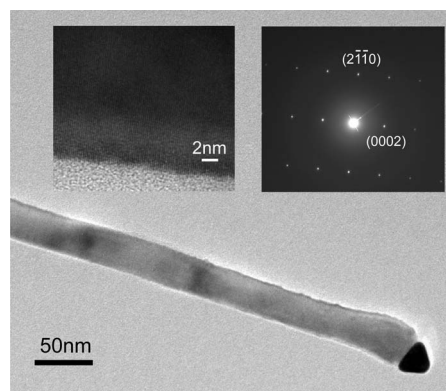


FIG. 1. TEM images and electron-diffraction patterns of a ZnO nanowire.

^{a)} Author to whom correspondence should be addressed. Electronic mail: yigu@wsu.edu.

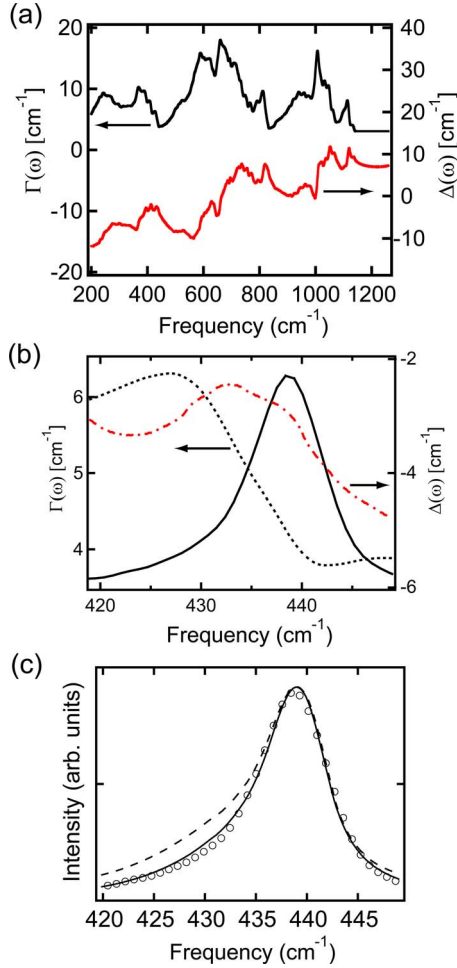


FIG. 2. (Color online) (a) $\Gamma(\omega)$ (black line) with $|V_3^+|^2$ and $|V_3^-|^2$ of 18 and 3 cm^{-2} , respectively, and $\Delta(\omega)$ (red line) calculated from the Kramers–Kronig relation; (b) experimental Raman spectrum of the E_2^{high} phonon (solid line), with $\Gamma(\omega)$ and $\Delta(\omega)$ plotted as black dashed and red dot-dashed lines, respectively; (c) simulated Raman line shape with $|V_3^+|^2$ of 18 cm^{-2} (solid line) and 28 cm^{-2} (dashed line), with $|V_3^-|^2$ of 3 cm^{-2} in both cases, together with the experimental Raman line shape (open circles).

$=550 \text{ cm}^{-1}$ and $\omega_4=110 \text{ cm}^{-1}$, respectively.^{5,10} This anharmonic phonon coupling changes the harmonic phonon frequency (ω_0) into a damped frequency ω , with $\omega=\omega_0+\Delta(\omega)+i\Gamma(\omega)$, where the term of $\Delta(\omega)+i\Gamma(\omega)$ is the phonon self-energy. The imaginary part of the phonon self-energy, $\Gamma(\omega)$, is given by¹¹

$$\Gamma(\omega) = |V_3^+|^2 \rho_+^{(2)}(\omega) [1 + n(\omega_1) + n(\omega_2)] + |V_3^-|^2 \rho_-^{(2)}(\omega) \times [n(\omega_4) - n(\omega_3)], \quad (1)$$

where $n(\omega)$ are Bose–Einstein occupation factors, $\rho_+^{(2)}(\omega)$ and $\rho_-^{(2)}(\omega)$ are the two-phonon sum and difference density of states (DOS), $|V_3^+|^2$ and $|V_3^-|^2$ are third-order anharmonic phonon coupling matrix elements for the decay into phonon sums and differences, respectively. The real part of the phonon self-energy, $\Delta(\omega)$, is related to $\Gamma(\omega)$ via the Kramers–Kronig transformation

$$\Delta(\omega) = -\frac{2}{\pi} \mathcal{P} \int_0^\infty \frac{\omega' \Gamma(\omega')}{\omega'^2 - \omega^2} d\omega', \quad (2)$$

where \mathcal{P} is the Cauchy principle value.

To evaluate the phonon self-energy, we used the two-phonon sum DOS reported in Ref. 10. We shifted the DOS by +10 cm^{-1} , as discussed in Refs. 6 and 10 for bulk ZnO, to compensate the errors in the *ab initio* calculations. For the two-phonon difference DOS, we used a constant value of 0.25 cm^{-1} (Ref. 5), as the DOS is almost flat in the frequency region of interest (400–460 cm^{-1}). Figure 2(a) shows the plot of $\Gamma(\omega)$ (black line) at RT calculated from Eq. (1), with $|V_3^+|^2$ and $|V_3^-|^2$ given by 18 and 3 cm^{-2} , respectively (see also below). We then used a numerical algorithm¹² to calculate $\Delta(\omega)$ [red line in Fig. 2(a)] via Eq. (2). The line shape of the Raman peak is then given by

$$I(\omega) \propto \frac{\Gamma(\omega)}{\Gamma(\omega)^2 + [\omega_0 + \Delta_0 + \Delta(\omega) - \omega]^2}, \quad (3)$$

where Δ_0 is the frequency shift due to the lattice thermal expansion

$$\Delta_0 = -\omega_0 \gamma \int_0^T [\alpha_{\parallel}(T') + 2\alpha_{\perp}(T')] dT', \quad (4)$$

with γ , $\alpha_{\parallel}(T)$, and $\alpha_{\perp}(T)$ being the Grüneisen parameter ($=2.02$),¹⁰ the linear thermal expansion coefficients parallel and perpendicular to the c axis, respectively. For α_{\parallel} and α_{\perp} , we used the values from Refs. 13 and 14 that extend from 90 to 400 K, and we extrapolated these values to the 80–600 K temperature regime.

The width of the Raman peak is determined, to a large extent, by $\Gamma(\omega)$. The asymmetric broadening is the result of the strong frequency dependence of $\Gamma(\omega)$ in the low-frequency tail region of the phonon peak, as shown in Fig. 2(b). Using Eqs. (1)–(4), we simulated the Raman line shape, with $|V_3^+|^2$ and $|V_3^-|^2$ as the two varying parameters. To account for the finite width of instrument response of $\sim 2 \text{ cm}^{-1}$, we have added this value to $\Gamma(\omega)$ during the simulation. The results, for $|V_3^+|^2=18 \text{ cm}^{-2}$ and $|V_3^-|^2=3 \text{ cm}^{-2}$, were plotted as the solid line in Fig. 2(c) that agrees well with the experimental Raman peak (open circles). Similar analysis performed on bulk ZnO (Ref. 6) has yielded $|V_3^+|^2 \approx 39 \text{ cm}^{-2}$ and $|V_3^-|^2 \approx 4\text{--}6 \text{ cm}^{-2}$. Values of 28 cm^{-2} for $|V_3^+|^2$, and 3 cm^{-2} for $|V_3^-|^2$, have been obtained⁵ on bulk ZnO via the relationship between the phonon linewidth and isotopic composition. While there is an agreement on the value of $|V_3^-|^2$, the obtained value (18 cm^{-2}) here for $|V_3^+|^2$ is noticeably lower than those (28–39 cm^{-2}) reported in bulk ZnO. We note that, as $\rho_-^{(2)}(\omega)$ is assumed to be a constant, $|V_3^-|^2$ mainly determines the symmetric broadening of the phonon peak, while larger values of $|V_3^+|^2$ indicates a larger degree of asymmetric broadening. To illustrate the significance of $|V_3^+|^2$, we simulated the Raman line shape [dashed line in Fig. 2(c)] using $|V_3^+|^2$ of 28 cm^{-2} , the lower end of the values reported in bulk ZnO. Obviously, the simulated line shape with $|V_3^+|^2$ of 28 cm^{-2} overestimates the asymmetric broadening of the E_2^{high} phonon peak observed in ZnO nanowires.

To further verify the validity of obtained values for $|V_3^+|^2$ and $|V_3^-|^2$, we calculated the peak position and the Raman linewidth as functions of temperature from the equations above, using the same values for $|V_3^+|^2$ and $|V_3^-|^2$. For the comparison to the experiments, we note that the measured Raman linewidth, the full width at half maximum (Γ_{FWHM}), is not simply $2\Gamma(\omega)$ but is given by¹¹

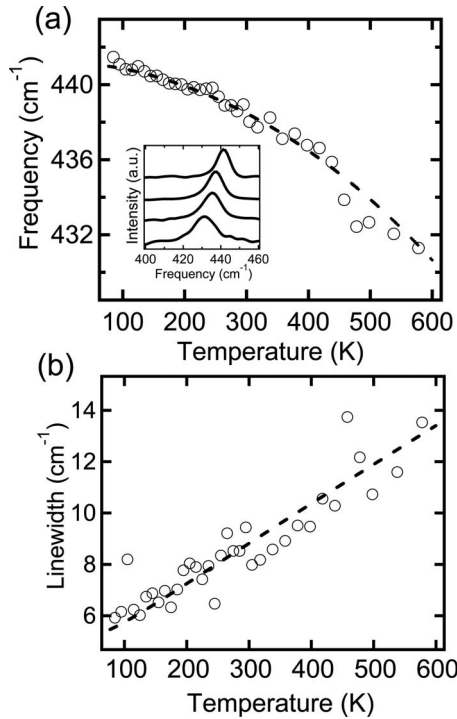


FIG. 3. Frequency (a) and linewidth (b) of the E_2^{high} phonon peak as functions of temperature. Open circles and dashed lines are experimental and calculated results, respectively. Inset to (a) shows the normalized Raman spectra obtained, from top, at 85, 320, 440, and 540 K, with spectra shifted vertically for clarity.

$$\Gamma_{\text{FWHM}} = \frac{2\Gamma(\omega_m)}{1 - \left. \frac{d\Delta(\omega)}{d\omega} \right|_{\omega=\omega_m}}, \quad (5)$$

where ω_m is the center frequency of the Raman peak. The calculated results (dashed lines) agree well with the experimental data (open circles) plotted in Fig. 3. This validates the values of $|V_3^+|^2$ and $|V_3^-|^2$ obtained via the Raman line shape analysis.

The lower value of $|V_3^+|^2$ obtained here suggests a suppressed anharmonic coupling of the E_2^{high} phonon to the sum of two acoustic phonons in VLS-grown ZnO nanowires compared to bulk ZnO. Given the diameter (~ 30 nm) of these nanowires, phonon confinement effects are not expected. In addition, Raman spectra of nanowires with diameters ranging from 20 to 80 nm (not shown here) exhibit no noticeable difference. Thus the size effect seems unlikely to be the origin. On the other hand, we note that the frequency of the two-phonon sum DOS $[\rho_+^{(2)}(\omega)]$ is inversely proportional to the Zn atomic mass.⁵ During the VLS growth, Zn atoms in the vapor phase are transported to the growth substrate and then diffuse through Au nanocatalysts before reacting with the oxygen. This process might lead to a preferred Zn isotopic composition (e.g., via isotope effects in intermetallic diffusion¹⁵) that is different than that of bulk ZnO. The resulting change in the magnitude (and the frequency depen-

dence) of $\rho_+^{(2)}(\omega)$ in the frequency region of the E_2^{high} phonon might account for the suppressed anharmonic phonon coupling. Further investigations are required to elucidate the underlying mechanisms.

In conclusion, via an analysis of the Raman phonon line shape, we quantitatively determined third-order anharmonic phonon coupling matrix elements in VLS-grown ZnO nanowires. The validity of these values was confirmed by variable-temperature Raman characteristics. The results suggest that the decay of the E_2^{high} phonon into the sum of two acoustic phonons is suppressed in VLS-grown ZnO nanowires compared to bulk ZnO. This can have profound effects on the mechanical as well as thermal properties of these nanomaterials. The origin of such a suppression might lie in the isotope effects on Zn vapor transport and diffusion through Au nanocatalysts during the VLS growth; further investigation are needed to identify the underlying mechanisms.

We thank Ashish Mishra at Washington State University and Dr. Chongmin Wang at Pacific Northwest National Laboratory (PNNL) for the TEM work, which was performed in the Environmental Molecular Sciences Laboratory, a national scientific user facility sponsored by DOE's Office of Biological and Environmental Research and located at PNNL. This work was supported by the National Science Foundation through the CAREER program (Grant No. DMR-0845007) and the Research Experience for Undergraduates program (Grant No. 0649023). Acknowledgment is made to the Donors of the American Chemical Society Petroleum Research Fund for partial support of this research.

¹B. M. Wen, J. E. Sader, and J. J. Boland, *Phys. Rev. Lett.* **101**, 175502 (2008).

²R. Agrawal, B. Peng, E. E. Gdoutos, and H. D. Espinosa, *Nano Lett.* **8**, 3668 (2008).

³A. J. Kulkarni, M. Zhou, K. Sarasamak, and S. Limpijumnong, *Phys. Rev. Lett.* **97**, 105502 (2006).

⁴X. D. Wang, J. H. Song, J. Liu, and Z. L. Wang, *Science* **316**, 102 (2007).

⁵J. Serrano, F. J. Manjon, A. H. Romero, F. Widulle, R. Lauck, and M. Cardona, *Phys. Rev. Lett.* **90**, 055510 (2003).

⁶R. Cusco, E. Alarcon-Llado, J. Ibanez, L. Artus, J. Jimenez, B. G. Wang, and M. J. Callahan, *Phys. Rev. B* **75**, 165202 (2007).

⁷A. Soudi, E. H. Khan, J. T. Dickinson, and Y. Gu, *Nano Lett.* **9**, 1844 (2009).

⁸Raman spectra with the 442 nm excitation (below the ZnO band gap) are dominated by the E_2^{high} phonon mode (a nonpolar mode), whereas the LO phonon modes (polar modes) become stronger with the 325 nm excitation (resonant with the ZnO band gap energy) due to the strong interaction between the electric dipoles associated with these phonon modes and photogenerated electron-hole pairs.

⁹F. Widulle, J. Serrano, and M. Cardona, *Phys. Rev. B* **65**, 075206 (2002).

¹⁰J. Serrano, A. H. Romero, F. J. Manjon, R. Lauck, M. Cardona, and A. Rubio, *Phys. Rev. B* **69**, 094306 (2004).

¹¹J. Menendez and M. Cardona, *Phys. Rev. B* **29**, 2051 (1984).

¹²Kramers-Kronig/Hilbert Transforms Procedure (http://www.wavemetrics.com/users/tools_KramersKronig.htm) implemented in IGOR (Wavemetrics, Lake Oswego, OR).

¹³B. Yates, R. F. Cooper, and M. M. Kreitman, *Phys. Rev. B* **4**, 1314 (1971).

¹⁴H. Ibach, *Phys. Status Solidi* **33**, 257 (1969).

¹⁵J. G. Mullen, *Phys. Rev.* **121**, 1649 (1961).